A low molecular weight mimic of the Toll/IL-1 receptor/resistance domain inhibits IL-1 receptor-mediated responses

Tamas Bartfai*†‡, M. Margarita Behrens*†, Svetlana Gaidarova*†, Janell Pemberton*†, Alexander Shivanyuk§¶, and Julius Rebek, Jr.‡§¶

Departments of *Neuropharmacology and §Chemistry, †The Harold L. Dorris Neurological Research Center, and ¶The Skaggs Institute for Chemical Biology, The Scripps Research Institute, 10550 North Torrey Pines Road, La Jolla, CA 92037

Contributed by Julius Rebek, Jr., May 7, 2003

Toll-like receptors (TLRs) and the type I IL-1 receptor (IL-1RI) are key components of the innate immune system activated by microbial infections and inflammation. The signaling cascade from agonist-occupied TLRs and IL-1Rs involves recruitment of the small cytosolic adapter protein MyD88 that binds to IL-1RI via homotypic interactions mediated by Toll/IL-1R/resistance (TIR) domains. Dominant negative forms and null mutations of MyD88 have recently been shown to preclude bacterial product or IL-1-mediated activation of NF-κB pathways, demonstrating that MyD88 is an essential component of the Toll receptor signaling. Here, we report the synthesis and pharmacological effects of a low molecular weight MyD88 mimic, hydrocinnamoyl-L-valyl pyrrolidine (compound 4a), modeled on a tripeptide sequence of the BB-loop [(F/Y)-(V/L/I)-(P/G)] of the TIR domain. Results are presented showing that compound 4a interferes with the interactions between mouse MyD88 and IL-1RI at the TIR domains. Compound 4a inhibited IL-1β-induced phosphorylation of the mitogen-activated protein kinase p38 in EL4 thymoma cells and in freshly isolated murine lymphocytes in a concentration-dependent manner. *In vivo*, compound 4a produced a significant attenuation of the IL-1β-induced fever response (200 mg/kg, i.p.). Inhibition of the TIR domain-mediated MyD88/IL1-RI interaction by a low molecular weight, cell-penetrating TIR domain mimic suggests an intracellular site for antiinflammatory drug action.

BB-loop | protein–protein interaction | IL-1β signaling | fever

Members of the Toll-like receptor (TLR)/IL-1 receptor superfamily play key roles in the activation of the innate immune system by bacterial components from Gram-negative and Gram-positive bacteria (1–3). The monomers of the heterodimeric proinflammatory cytokine receptor, the IL-1 type I receptor (IL-1RI), and the IL-1R accessory protein (IL-1RAcP) are members of this superfamily that on ligand binding initiate intracellular signaling by dimerization and recruitment of the adapter protein MyD88 through homotypic binding of a cytosolic recognition domain [Toll/IL-1R/resistance (TIR) domain] between IL-1RI and MyD88 (4, 5). MyD88 is composed of an N-terminal death domain (DD), an intermediate region (ID), and a C-terminal TIR domain (6). MyD88 homodimers are thought to be associated via interaction between DD and TIR–TIR domains. TIR–TIR interactions of MyD88 with the agonist occupied IL-1RI on the one hand and with the downstream interleukin receptor-associated kinase (IRAK) on the other are thought to mediate IL-1β signaling (7).

MyD88 seems to play a key role in the transduction of infectious and inflammatory signals from TLR/IL-1Rs to the activation of gene transcription via NF-κB activation (2). The expression levels of MyD88 and its differential splicing regulate important phenomena such as endotoxin tolerance (8, 9), or IFN-γ and granulocyte-macrophage colony-stimulating factor (GM-CSF) actions (10). Evolution, transgenic, and molecular biological experiments point to MyD88 as a pivotal element in signal transduction from the TLR/IL-1R family: pox viruses like vaccinia express A46R and A52R proteins that have dominant negative effects on MyD88 recruitment and block TIR-mediated signaling in the host (11). MyD88$^{-/-}$ animals lack all responses to IL-1 (12), and show lowered resistance to *Toxoplasma gondii* infection (13). Furthermore, expression of the dominant negative form of MyD88 blocked IL-1-induced NF-κB activation in several cellular models (6). However, MyD88 is not the only adapter protein that can transduce lipopolysaccharide (LPS) signals. Recently, adapter proteins such as Mal/Tirap have been shown to mediate LPS-induced signaling cascades even in the absence of MyD88 (14, 15).

The importance of the TIR domain-mediated homotypic interaction between TLRs and MyD88 is best demonstrated by a point mutation (P712H) in the TIR domain of TLR4 (the LPS receptor). This mutation, by preventing the recruitment of adapter proteins, renders mice carrying the P712H point mutation endotoxin resistant (16).

The structural basis for TIR-mediated homotypic interactions was elucidated by x-ray structure of the TIR domain of human TLR2, consisting of five-stranded parallel β-sheets and of five surrounding α-helices interconnected by loops (17). A large conserved surface, involving the BB-loop with consensus sequences (F/Y)-(V/L/I)-(P/G) in different Toll receptors and MyD88 homologs, emerges as key to the TIR domain-mediated homotypic protein–protein interaction.

We have synthesized analogs of the central 3-aa sequence of the BB-loop and studied their effect on IL-1RI signaling *in vitro* and *in vivo*. The first active compound, hydrocinnamoyl-L-valyl pyrrolidine (**4a** in Fig. 1), showed that it is possible to mimic the *in vitro* and *in vivo* effects of the dominant negative form of MyD88, or of the extracellular binding IL-1R antagonist in blocking IL-1RI-mediated signaling. The ability of this relatively small molecule to regulate protein–protein interactions is of note. These findings may also be of pharmacological importance because the blockade of IL-1 signaling has therapeutic effects in rheumatic arthritis and sepsis as shown by the recently introduced IL-1R antagonist (Kinneret) in clinical practice.

Methods

Synthesis of TIR/BB-Loop Mimics. ***Synthesis of 2a.*** Pyrrolidine (3 ml, 36 mmol) was added to a solution of commercial BOC-L-valine-hydroxysuccinimide ester (**1a**; 1.5 g, 4.77 mM) in toluene (15 ml). The reaction mixture was stirred at ambient temperature for 8 h. The precipitate was filtered, and the filtrate was evaporated at reduced pressure. The remaining oil was dissolved in dichlo-

Abbreviations: TLR, Toll-like receptor; IL-1RI, type I IL-1 receptor; IL-1RAcP, IL-1R accessory protein; TIR, Toll/IL-1R/resistance; LPS, lipopolysaccharide; DCM, dichloromethane; MAP, mitogen-activated protein; ERK, extracellular signal-regulated kinase; JNK, c-Jun amino-terminal kinase.

‡To whom correspondence should be addressed. E-mail: tbartfai@scripps.edu or jrebek@scripps.edu.

PHARMACOLOGY

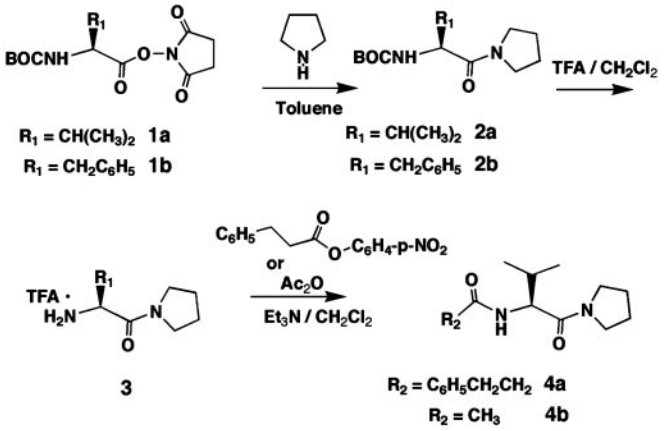

Fig. 1. Synthesis of BB-loop mimic based on the [(F/Y)-(V/L/I)-(P/G)] consensus sequence in TIR domains of TLRs, IL-1RI, and MyD88.

romethane (DCM; 50 ml), and the solution was washed with water (3 × 50 ml) to remove the traces of hydroxysuccinimide. The organic layer was evaporated, and, after drying *in vacuo* for 48 h, the oil crystallized. Yield 89%. Mp 49°C. ^{1}H NMR (600 MHz, $CDCl_3$): δ = 5.27 ppm (d,J = 9.5 Hz, 1H), 4.28–4.23 (m, 1H), 3.72–3.62 (m, 1H), 3.57–3.39 (m, 1H), 2.10–1.82 (m, 5H), 1.44 (s, 9H), 0.97 (d,J = 6.6 Hz, 3H), 0.94 (d,J = 7.3 Hz, 3H).

Synthesis of 2b. Compound **2b** was prepared similarly to **2a**, starting from BOC-L-phenylalanine-hydroxysuccinimide ester. Yield 85%. Mp 56°C. ^{1}H NMR (600 MHz, $CDCl_3$):δ 7.30–7.18 (m, 5H), 5.39 (d,J = 8.8 Hz, 1H), 4.62–4.55 (m, 1H), 3.70–3.27 (m, 3H), 3.03–2.90 (m, 2H), 2.59–2.57 (m, 1H), 1.79–1.70 (m, 2H), 1.67–1.61 (m, 1H), 1.42 (s, 9H).

Synthesis of 3. Trifluoroacetic acid (10 ml) was added to a solution of **2a** (0.9 g, 0.33 mol) in dry DCM (20 ml). The reaction mixture was stirred for 4 h at ambient temperature, then was diluted with toluene (100 ml) and evaporated at reduced pressure. The residue was dried *in vacuo* for 24 h and remained as a colorless oil as the monotriflate. Yield 100%. ^{1}H NMR (600 MHz, $CDCl_3$): δ 8.2 (br. s, 3H), 4.02 (d,J = 5.9 Hz, 1H), 3.65–3.58 (m, 1H), 3.46–3.33 (m, 1H), 3.46–3.33 (m, 2H), 2.24–2.15 (m, 1H), 2.03–1.80 (m, 4H), 1.10 (d,J = 7.3 Hz, 3H) 1.06 (d,J = 6.6 Hz, 3H).

Synthesis of 4a. The amine triflate **3** (0.9 g, 3.4 mmol) was dissolved in dry DCM (10 ml). Triethylamine (2 ml) was added to this solution followed by hydrocinnamoyl *p*-nitrophenolate (1.4 g, 5.1 mmol) dissolved in DCM (5 ml). The reaction mixture was stirred at ambient temperature overnight and thereafter evaporated. The residue was dissolved in tetrahydrofuran (30 ml), and water (10 ml) and triethylamine (5 ml) were added to destroy the excess *p*-nitrophenyl ester. The solution was stirred for 8 h at ambient temperature and then diluted with DCM. The organic phase was washed with water until the aqueous layer was colorless. The organic layer was separated and then evaporated *in vacuo*. The slightly yellowish oil was dried *in vacuo* for 24 h. Yield 67%. ^{1}H NMR (600 MHz, $CDCl_3$): δ 7.34–7.18 (m, 5H), 6.10 (d,J = 8.8 Hz, 1H), 4.60 and 4.59 (two d,J = 7.3 Hz, J = 6.6 Hz, 1H), 3.73–3.68 (m, 1H), 3.53–3.39 (m, 3H), 3.02–2.92 (m, 2H), 2.58–2.48 (m, 2H), 1.99–1.82 (m,5H), 0.91 (d,J = 6.6 Hz, 3H), 0.82 (d,J = 7.3 Hz, 3H).

Synthesis of 4b. The amine triflate **3** (0.9 g, 3.4 mmol) was dissolved in acetic anhydride (10 ml), and triethylamine (1 g) was added. The reaction mixture was stirred at ambient temperature for 8 h and evaporated *in vacuo*. The residue was dissolved in toluene (50 ml), and the solution was evaporated. This procedure was repeated three times to assure the removal of triethylamine and trifluoroacetic acid. The resulting oil was dried *in vacuo* for 96 h, and after standing it crystallized. Yield >90%. Mp 56°C. ^{1}H-NMR (600 MHz, $CDCl_3$): δ 6.17 (d,J = 8.8 Hz, 1H), 4.62 and 4.60 (two d,J = 7.3 Hz, 1H), 3.75–3.69 (m, 1H), 3.55–3.39 (m, 3H), 2.01 (s, 3H) 2.00–1.83 (m, 5H), 0.97 (d,J = 6.6 Hz, 3H), 0.94 (d,J = 7.3 Hz, 3H).

The 1D NMR spectra were recorded on a Bruker (Billerica, MA) DRX 600 (600 MHz) spectrometer by using the solvent signals as internal reference. Crystallographic data were collected on a Siemens (Iselin, NJ) SMART (18) diffractometer equipped with a charge-coupled device area detector by using graphite monochromatized MoK_α radiation [$\lambda(MoK_\alpha)$ = 0.71073 Å]. Data in the frames corresponding to an arbitrary hemisphere of data were integrated by using SAINT (19). Data were corrected for Lorentz and polarization effects and were further analyzed by using XPREP. An empirical absorption correction based on the measurement of redundant and equivalent reflections and an ellipsoidal model for the absorption surface was applied by using SADABS. The structure solution and refinement were performed by using SHELXTL (refining on F^2) (20).

Crystallographic Details for 4b. Monoclinic, $P2_1$, a = 9.763(4) Å, b = 13.051(5) Å, c = 10.561(4) Å, β = 113.492(7)°, V = 1234.2(8) Å^3, Z = 2, ρ = 1.327 g·cm^{-3}, μ = 0.09 cm^{-1}, $2\theta_{max}$ = 56.48°, R1 = 0.0643, wR2 = 0.1431 [for 1,637 reflections, I > 2σ(I)], R1 = 0.170, wR2 = 0.1943 (for 3,844 independent reflections), 277 parameters, S = 0.956, $\Delta\rho$ (max/min) = 0.19/−0.20 eÅ^{-3}.

Cell Culture. EL4 murine thymoma cells (American Type Culture Collection no. TIB-39) were grown in DMEM supplemented with 10% FBS, 4 mM glutamine, and 2 mM Pen-Strep (GIBCO). Cells were washed in the medium above without serum, and resuspended at a cell density of 3–4 × 10^6 per ml in the absence of serum, and returned to the incubator for 4 h to allow recovery.

For spleen cell isolation, spleens from 10–12 mice were aseptically removed and collected in cold PBS. Spleens were then positioned in a 100-mm Petri dish and thoroughly grinded with the flat part of a syringe in 5 ml of RPMI medium 1640, supplemented with 58 mg/liter glutamine and 10 units/liter penicillin. After connective tissue removal, the cell suspension was transferred on top of a 3-ml layer of Ficoll-Plaque Plus (Amersham Pharmacia Biosciences), and centrifuged at 100 × g for 20 min at room temperature. Lymphocyte fraction was finally resuspended in RPMI medium 1640, and allowed to recover for 4–16 h before experiments.

Cell Exposures and Protein Extract Preparation. Murine IL-1β (R & D Systems) and LPS (Sigma) were dissolved in sterile double distilled water, and **4a** was dissolved in DMSO. After serum deprivation, either EL4 cells or spleen cells were exposed to varying concentrations of **4a** for 15 min before IL-1β (10 nM) exposure or LPS (10 ng/ml) exposure. Time course experiments (0–30 min) showed that maximal mitogen-activated protein (MAP) kinase phosphorylation occurred at 15 min and 30 min for IL-1β and LPS incubations, respectively. These exposure times were used throughout the studies. After IL-1β or LPS exposure, EL4 cells or freshly isolated lymphocytes were centrifuged and washed once with ice cold PBS, and resuspended in ice cold lysis buffer (1% Nonidet P-40/20 mM Tris·Cl, pH 7.5/10 mM EGTA/40 mM β-glycerolphosphate/2.5 mM $MgCl_2$/2 mM orthovanadate/1 mM DTT/1 mM PMSF/20 μg/ml aprotinin/20 μg/ml leupeptin) and processed as described (21). Protein concentration was determined by using the bicinchoninic acid method (BCA, Pierce).

Western Blot Analysis. For the study of p38, extracellular signal-regulated kinase (ERK) 1/2, and c-Jun amino-terminal kinase (JNK) MAP kinases, 40 μg of protein samples were fractionated

on 8% SDS/PAGE, and transferred to nitrocellulose membranes (Micron Separations, Westboro, MA) by using a semidry electrotransfer system (Novablot, Amersham Pharmacia). Membranes were blocked with 5% milk in TBS-T buffer (20 mM Tris, pH 7.5/150 mM NaCl/0.05% Tween 20), and were then incubated with phospho-specific antibodies directed to the phosphorylated forms of p38, ERK1/2, and JNK (Cell Signaling Technology, Beverly, MA). Protein bands were visualized by chemiluminescence using SuperSignal (Pierce). For densitometric analysis and quantification, blots were subsequently reprobed with specific antibodies directed to non-phospho form of p38, ERK1/2, and JNK (Santa Cruz Biotechnology). In parallel experiments for p38 MAP kinase phosphorylation determinations, a commercially available ELISA system was also employed (BioSource International, Camarillo, CA), using 10 μg of total cell lysate. Results were calculated as absorbance per μg of protein and expressed as a percentage of the basal value (in the absence of any exposure).

Immunoprecipitation and Sandwich ELISA. For coimmunoprecipitation experiments, 80 μg of total cell lysate were incubated with 20 μl of anti-MyD88-conjugated agarose (Santa Cruz Biotechnology) over night at 4°C, washed three times in PBS, and resuspended in Laemmli sample buffer. Proteins were separated in 10% SDS/PAGE, and coimmunoprecipitating bands were detected by Western blot using specific antibodies (anti-IL-1RI and TLR4 from Santa Cruz). As a control, counter immunoprecipitations were also performed. For the development of the sandwich ELISA system, 96-well plates were coated overnight with anti-MyD88 antibody (2 mg/ml in bicarbonate/PBS buffer, pH 7.5). Plates were washed of excess antibody in PBS-Tween 20, protein extracts (10 μg) were added, and incubation was allowed for 16–24 h at 4°C. Plates were again washed as above, and anti-IL-1RI (1 μg/ml) or TLR4 (1 μg/ml) was added for 2 h at room temperature. Plates were washed, and a secondary antibody conjugated to horseradish peroxidase (1:2,000, Vector Laboratories) was added and incubated at room temperature for 1 h. After washing with PBS, color was developed by using commercially available reagents (Biosource International) and read in a Bio-Rad plate reader at 450 nm. As controls, incubations were performed in the absence of each of the antibodies, one at a time, and in the absence of cell extract, which was considered the blank, and subtracted from the values obtained. Values were calculated as absorbance per μg of protein, and expressed as a percentage of basal (control) conditions.

Densitometric Analysis and Quantification. The intensity of immunoreactive bands obtained in autoradiographic films was measured with an imaging densitometer (Bio-Rad). Phosphoprotein levels per protein unit ratios were obtained by dividing the phospho-immunoreactive densitometry values by those obtained for the respective protein redetection blots. All values were expressed as a percentage of basal levels for each experiment.

Fever Studies. Radiotelemetric devices from Data Sciences International (Minneapolis) were implanted i.p. into adult male C57BL/6 mice 1 wk before experiments. The mice recovered in a thermo-neutral room maintained at 31.5°C. The basal temperature recordings were performed for 24 h before initiation of experiments. At 10:30 a.m. the day of the experiment, saline or **4a** (diluted in saline; 200 mg/kg) was injected i.p. At 10:45 a.m., rmIL-1β (15 μg/kg; R & D Systems) or saline was injected i.p. The core body temperature was continuously recorded for the following 24 h. The fever data obtained in the absence and presence of **4a** was analyzed by ANOVA followed by Tukey test.

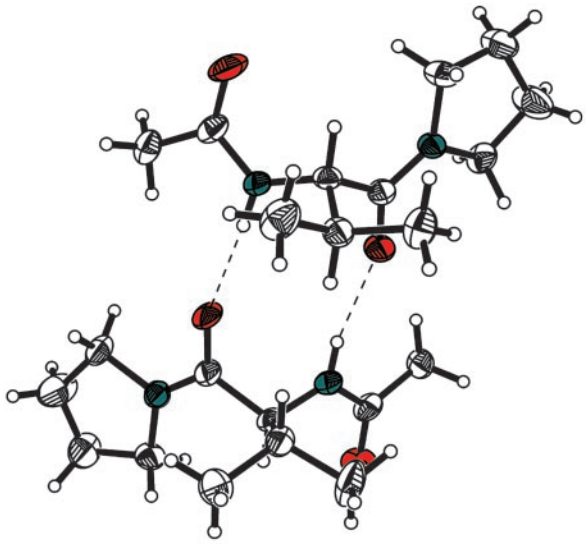

Fig. 2. Crystal structure of acetamide **4b** in Ortep presentation (20% occupation thermal ellipsoids). Both crystallographically independent molecules are shown. Hydrogen bonds are indicated by dotted lines.

Results

Synthesis of TIR/BB-Loop Mimics. The synthesis proceeded uneventfully through use of standard coupling and deprotection techniques. Reaction of commercially available BOC-L-valine hydroxysuccinimide ester **1a** (Fig. 1) with pyrrolidine in toluene in the presence of triethylamine afforded amide **2a** in ≈90% yield. Analogous reaction of the phenylalanine ester **1b** gave compound **2b**. Removal of the BOC group by trifluoroacetic acid in dichloromethane resulted in the corresponding amine **3**. Acylation of **3** with *p*-nitrophenylhydrocinnamate in toluene afforded amide **4a** as heavy oil. Acylation of **3** with acetic anhydride resulted in acetamide **4b** that crystallized on drying *in vacuo*.

Stable crystals suitable for the single crystal x-ray analysis were obtained. Two crystallographically independent molecules are found in the asymmetric unit that forms a dimer through two hydrogen bonds between the NH groups and the valine carbonyls (Fig. 2). No deviations from the regular bond lengths and angles were detected in the crystalline state.

Biological Effects of TIR/BB-Loop Mimics. As a central proinflammatory mediator, IL-1 induces the expression of multiple genes involved in the inflammatory process. IL-1 binds to IL-1RI, after which the receptor forms a complex with IL-1RAcP. This result triggers the recruitment of the adaptor protein MyD88, which associates with IL-1RI through its carboxyl-terminal TIR domain. Once recruited to the IL-1R complex, MyD88 activates the interleukin receptor-associated kinases 1–4 (IRAK1 to -4), which become phosphorylated and dissociate from MyD88 and associate with the tumor necrosis factor receptor-associated factor 6 (TRAF6), leading to the activation of the MAP kinases p38, ERK1/2, and JNK) and the activation of IκB, which induces the activation of transcription factor NF-κB. Similarly, LPS binding, via CD14, to TLR4 induces the recruitment of MyD88 and triggering of the same signaling cascade as IL-1β binding to IL-1RI (1).

To analyze the effects of TIR/BB-loop mimics on IL-1RI-mediated signaling, we used the activation of the MAP kinase p38, for which reliable phospho-specific antibodies and ELISA systems have been developed. Activation of p38 MAP kinase occurs through dual (Thr, Tyr) phosphorylation of the tripeptide Thr-Gly-Tyr by MAP kinase kinases 3 and 6, producing a fully

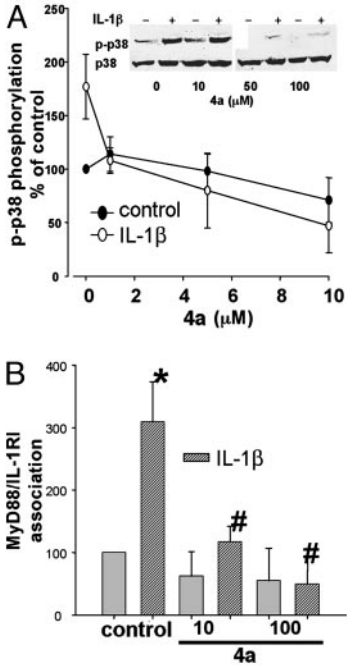

Fig. 3. **4a** attenuates IL-1β-mediated activation of p38 MAP kinase and prevents IL-1β-mediated IL-1RI/MyD88 association in EL4 cells. (*A*) EL4 cells, preincubated for 15 min in the absence or presence of varying concentrations of **4a** (0–100 μM), were exposed to either IL-1β (10 nM, ○) or water (●) for an additional 15 min. Cells were lysed as described in *Methods*, and proteins were separated by SDS/PAGE and processed for Western blots by using anti-phospho-p38 MAP kinase antibody. Membranes were subsequently stripped and incubated with non-phospho-p38 MAP kinase antibodies. Values were calculated as ratios of phospho/non-phospho form, and are expressed as a percentage of nontreated cells (control without **4a**). $n = 5$ independent experiments. *, Statistical significance over control plus IL-1β at $P < 0.05$ by ANOVA followed by Tukey test. (*B*) Cells were treated as in *A*, and 10 μg of protein extracts were subjected to a sandwich ELISA (see *Methods*) to analyze the effects of **4a** in the association of IL-1RI and MyD88. ELISAs were performed in triplicate, and data are cumulative for five independent experiments. Values were calculated as a percentage of control. The * indicates statistical significance with respect to control, and the # indicates statistical significance with respect to IL-1β at $P < 0.05$ by ANOVA followed by Tukey test.

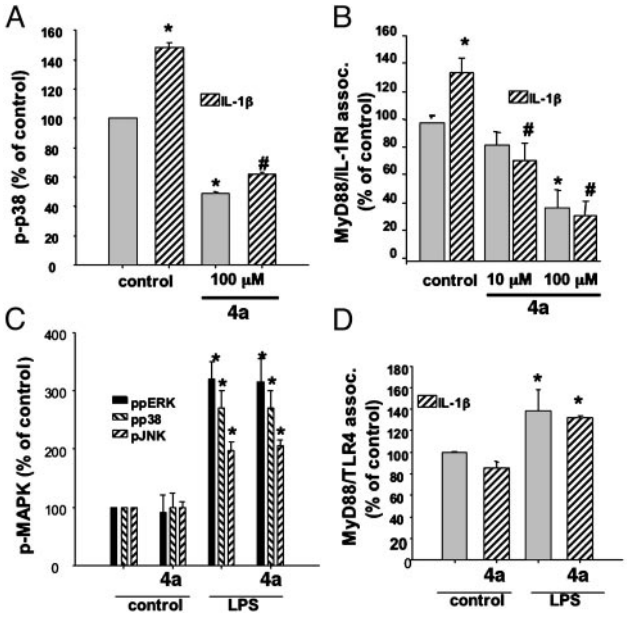

Fig. 4. **4a** attenuated IL-1β-mediated, but not LPS-mediated, effects in freshly isolated lymphocytes. Freshly isolated murine lymphocytes were treated similarly as EL4 cells with either IL-1β (*A* and *B*) or LPS (10 ng/ml, 30 min; *C* and *D*). MAP kinase activation (*A* and *C*) and the association of MyD88 with either IL-1RI (*B*) or TLR4 (*D*) were analyzed as described in Fig. 1. $n = 3$–8 independent experiments. The * indicates statistical significance with respect to control, and the # indicates statistical significance with respect to IL-1β at $P < 0.05$ by ANOVA followed by Tukey test.

active kinase (22). Antibodies specific to the dual-phosphorylated p38-enzyme have been proven as an efficient tool to analyze the activation state of this MAP kinase on activation of a broad spectrum of membrane receptors.

In mouse thymoma EL4 cells, a 15-min preincubation with **4a** (0–100 μM) inhibited IL-1β (10 nM)-mediated phosphorylation of p38 MAP kinase, where **4a** concentrations above 10 μM showed statistical significance (Fig. 3). To analyze the specificity of **4a** effect in preventing IL-1RI/MyD88 association, we performed coimmunoprecipitation and sandwich-ELISA assays by using antibodies specific for MyD88 and IL-1RI. IL-1β exposure of EL4 cells induced a significant increase in MyD88/IL-1RI association when analyzed both by sandwich ELISA (Fig. 3*B*) and coimmunoprecipitation assays using MyD88-specific antibody followed by Western blots with IL-1RI antibody (not shown). It should be noted that the sandwich ELISA system gave more reliable results than the coimmunoprecipitation assay, probably due to the higher amount of antibody and protein extract needed to perform the immunoprecipitation and Western blot redetection. The IL-1β-mediated association of MyD88/IL-1RI was prevented by preincubation of EL4 cells with **4a** (10–100 μM; Fig. 3*B*). To further prove the effects of **4a** on MyD88/IL-1RI association and prevention of IL-1β signaling, we performed similar experiments as those in EL4 cells in freshly isolated lymphocytes from mouse spleen. When IL-1β (10 nM)-mediated activation of p38 MAP kinase was analyzed in lymphocytes, **4a** showed similar inhibitory effects as in EL4 cells (Fig. 4*A*). When the association of MyD88/IL-1RI in freshly isolated lymphocytes was analyzed, **4a** showed inhibitory effects on the protein–protein interaction in the same concentration range as that observed for EL4 cells (Fig. 4*B*).

MyD88 has been shown to participate in signaling not only by IL-1RI but also through other members of the Toll receptor superfamily (TLR1 to -10; ref. 1). To analyze whether the inhibitory effects of **4a** were specific for IL-1β signaling, and thus to IL-1RI/MyD88 interaction, or they extended to other members of the Toll receptor family, we studied the effects of **4a** on LPS signaling in freshly isolated lymphocytes. LPS has been shown to bind to CD14 and TLR4, which, by recruiting MyD88, initiate signaling cascades similar to those elicited by IL-1β binding to IL-1RI/IL-1RAcP, i.e., MAP kinases p38, ERK1/2, and JNK, as well as the activation of the transcription factor NF-κB. Addition of LPS (10 ng/ml) to freshly isolated lymphocytes induced a robust activation of the three MAP kinase pathways (Fig. 4*C*). However, addition of **4a** (100 μM) did not have any effect on the activation state of these MAP kinases. Moreover, **4a** (100 μM) did not affect the association of TLR4/MyD88 (Fig. 4*D*), demonstrating the specificity of **4a** for the association of IL-1RI with MyD88.

As a further proof of the effects of **4a** on IL-1β signaling, we analyzed the TIR/BB-loop mimic in a well-established paradigm *in vivo*: the IL-1β-induced fever response. As previously demonstrated, injection of IL-1β (15 μg/kg) i.p. induced a fever response that peaks at ≈2 h postinjection, and lasts ≈6 h (Fig. 5). **4a** (200 mg/kg) applied i.p. 15 min before IL-1β injection attenuated this fever response (Fig. 5). Of note, the handling effect on the core body temperature, which has been shown to be independent of IL-1β (23), was not affected by **4a**, again

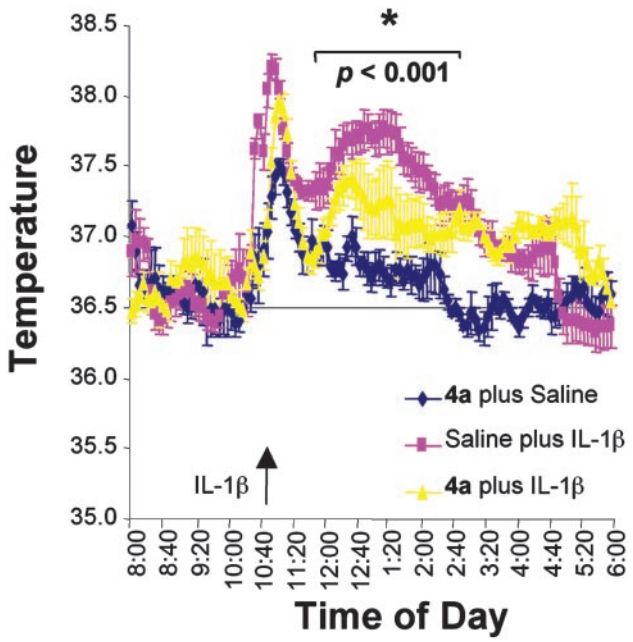

Fig. 5. **4a** attenuates IL-1β-induced fever in mice. Radiotelemetric devices were implanted in C57BL/6 male mice 2 wk before experiments. At 10:30 a.m. the day of the experiment, saline or **4a** (diluted in saline, 200 mg/kg) was injected i.p. At 10:45 a.m., rmIL-1β (15 μg/kg; R & D Systems) or saline was injected i.p (arrow). The core body temperature was recorded at 5-min intervals for the following 24 h. Statistical analysis of the temperature data obtained in the absence and presence of **4a** was performed by using one-way ANOVA followed by the Tukey test. $n = 4$ animals per group. *, Statistical significance of values obtained in the presence of **4a** with respect to saline plus IL-1β at $P < 0.001$.

demonstrating the specificity of the inhibitory effects of the TIR/BB-loop mimic **4a** for IL-1β mediated effects.

Discussion

The TIR–TIR domain-mediated homotypic interactions play a key role in Toll receptor signaling in the innate immune system. The presence of TIR domains on Toll receptors that respond to microbial components, on the receptor for the proinflammatory cytokine IL-1, and on the cytosolic adapter protein MyD88 that mediates the signals to interleukin receptor-associated kinase kinase suggests that disruption of TIR–TIR signaling would be of therapeutic value in the treatment of infectious and inflammatory diseases.

The structural basis of homotypic TIR–TIR domain interactions in the case of human TLR2 proposed by Xu and colleagues (17) shows that a 5-aa-long BB-loop in the middle of the five β-strand, five α-helix, 110-aa-long TIR domain is key to the interaction between the large conserved surfaces. The affinity of this interaction was estimated to be low (10^{-3} to 10^{-5} M). We show here that a low molecular weight mimic of the three protruding amino acids in the BB-loop [(F/Y)-(V/L/I)-(P/G)] (consensus for several IL-1RI, MyD88, and Toll receptors) can successfully inhibit interactions between IL-1RI and MyD88. Whereas there is no structural evidence that the hydrocinnamoyl group assumes the role of the F in the sequence, the crystal structure of the close **4a** analog (compound **4b**, Fig. 2) shows a conformation typical of a β-strand and that of the BB-loop. Moreover, **4b** forms a dimeric structure in the solid state, as might be expected of a mimic of structures involved in homotypic dimerization. The inhibition of this protein–protein interaction upstream in the IL-1 signaling pathways blocks IL-1-mediated *in vitro* and *in vivo* responses, similarly to the dominant negative form of MyD88.

Although the lack of effect of **4a** in the LPS-mediated activation of MAP kinase signaling cascades could be attributed to the activation of these cascades by other adapter proteins, as was shown for MyD88-deficient mice (14), **4a** showed no inhibitory effect on the interaction between TLR4 and MyD88. The specificity shown by the small BB-loop mimic reported here for the IL-1R/MyD88 interaction over those of TLR4/MyD88 suggests that the different TIR domain-mediated interactions may be amenable to inhibition by relatively low molecular weight, cell penetrating, and systemically active compounds. Further, the amino acid variations between the BB-loops in TIR domains of different TLRs hint at the possibility of specific pharmacological targeting of a given TLR signaling pathway, given the sequence variations in TIR domains of MyD88 and MyD88-like adapter proteins and those of the TIR domains of the TLRs. In a broader context, the example of **4a** provides additional evidence for the regulation of protein–protein interactions through mimics of the appropriate protein surfaces created by chemical synthesis. Indeed, the past years have witnessed the start of a trend in synthesizing nonpeptidic small molecule-mimics that can inhibit protein–protein interaction or mimic one of the interacting proteins (24). Thus, low molecular weight agonists for EPO receptor (25) and insulin receptor tyrosine kinase (26), as well as inhibitors of chemokine–chemokine receptor interaction (27) and Myc/Max dimerization (28), were described. The present work adds another example to the list of small molecules that can specifically interfere with protein–protein interaction.

This work was supported by The Skaggs Institute for Research, National Institutes of Health Grant AI50900 (to J.R.), The Harold Dorris Foundation, and The Ellison Foundation (to T.B.). A.S. is a Skaggs Postdoctoral Fellow.

1. Dunne, A. & O'Neill, L. A. J. (February 25, 2003) *Sci. STKE*, 10.1126/stke.2003.171.re3.
2. Janssens, S. & Beyaert, R. (2002) *Trends Biochem. Sci.* **27,** 474–482.
3. O'Neill, L. (2000) *Biochem. Soc. Trans.* **28,** 557–563.
4. Lord, K. A., Hoffman-Liebermann, B. & Liebermann, D. A. (1990) *Oncogene* **5,** 1095–1097.
5. Medzhitov, R., Preston-Hurlburt, P., Kopp, E., Stadlen, A., Chen, C., Ghosh, S. & Janeway, C. A., Jr. (1998) *Mol. Cell* **2,** 253–258.
6. Janssens, S., Burns, K., Tschopp, J. & Beyaert, R. (2002) *Curr. Biol.* **12,** 467–471.
7. Burns, K., Martinon, F., Esslinger, C., Pahl, H., Schneider, P., Bodmer, J. L., Di Marco, F., French, L. & Tschopp, J. (1998) *J. Biol. Chem.* **273,** 12203–12209.
8. Medvedev, A. E., Lentschat, A., Wahl, L. M., Golenbock, D. T. & Vogel, S. N. (2002) *J. Immunol.* **169,** 5209–5216.
9. Li, L., Cousart, S., Hu, J. & McCall, C. E. (2000) *J. Biol. Chem.* **275,** 23340–23345.
10. Adib-Conquy, M. & Cavaillon, J. M. (2002) *J. Biol. Chem.* **277,** 27927–27934.
11. Bowie, A., Kiss-Toth, E., Symons, J. A., Smith, G. L., Dower, S. K. & O'Neill, L. A. (2000) *Proc. Natl. Acad. Sci. USA* **97,** 10162–10167.
12. Adachi, O., Kawai, T., Takeda, K., Matsumoto, M., Tsutsui, H., Sakagami, M., Nakanishi, K. & Akira, S. (1998) *Immunity* **9,** 143–150.
13. Scanga, C. A., Aliberti, J., Jankovic, D., Tilloy, F., Bennouna, S., Denkers, E. Y., Medzhitov, R. & Sher, A. (2002) *J. Immunol.* **168,** 5997–6001.
14. Kawai, T., Adachi, O., Ogawa, T., Takeda, K. & Akira, S. (1999) *Immunity* **11,** 115–122.
15. O'Neill, L. A. (2002) *Trends Immunol.* **23,** 296–300.
16. Poltorak, A., He, X., Smirnova, I., Liu, M. Y., Van Huffel, C., Du, X., Birdwell, D., Alejos, E., Silva, M., Galanos, C., *et al.* (1998) *Science* **282,** 2085–2088.
17. Xu, Y., Tao, X., Shen, B., Horng, T., Medzhitov, R., Manley, J. L. & Tong, L. (2000) *Nature* **408,** 111–115.
18. Anonymous (1995) SMART, Area Detector Software Package (Siemens Industrial Automation, Madison, WI).
19. Anonymous (1995) SAINT, SAX Area Detector Integration Program (Siemens Industrial Automation, Madison, WI).

20. Sheldrick, G. (1993) SHELXTL (Siemens Industrial Automation, Madison, WI).
21. Behrens, M. M., Strasser, U., Koh, J. Y., Gwag, B. J. & Choi, D. W. (1999) *Neuroscience* **94,** 917–927.
22. Kyriakis, J. M. & Avruch, J. (2001) *Physiol. Rev.* **81,** 807–869.
23. Chai, Z., Alheim, K., Lundkvist, J., Gatti, S. & Bartfai, T. (1996) *Cytokine* **8,** 227–237.
24. Cochran, A. G. (2001) *Curr. Opin. Chem. Biol.* **5,** 654–659.
25. Qureshi, S. A., Kim, R. M., Konteatis, Z., Biazzo, D. E., Motamedi, H., Rodrigues, R., Boice, J. A., Calaycay, J. R., Bednarek, M. A., Griffin, P., *et al*. (1999) *Proc. Natl. Acad. Sci. USA* **96,** 12156–12161.
26. Salituro, G. M., Pelaez, F. & Zhang, B. B. (2001) *Recent Prog. Horm. Res.* **56,** 107–126.
27. Rajarathnam, K. (2002) *Curr. Pharm. Des.* **8,** 2159–2169.
28. Berg, T., Cohen, S. B., Desharnais, J., Sonderegger, C., Maslyar, D. J., Goldberg, J., Boger, D. L. & Vogt, P. K. (2002) *Proc. Natl. Acad. Sci. USA* **99,** 3830–3835.